Simulations and concepts for a 2-D spin-echo modulated SANS (SEMSANS) instrument

Parnell, Steven R.; Berg, Sergi Van Den; Bolderink, Gregor; Bouwman, Wim G.

DOI
10.1088/1742-6596/2481/1/012007

Publication date
2023

Document Version
Final published version

Published in
Journal of Physics: Conference Series

Simulations and concepts for a 2-D spin-echo modulated SANS (SEMSANS) instrument

Simulations and concepts for a 2-D spin-echo modulated SANS (SEMSANS) instrument

Steven R. Parnell, Sergi Van Den Berg, Gregor Bolderink and Wim G. Bouwman

Faculty of Applied Sciences, Delft University of Technology, Mekelweg 15, 2629 JB Delft, The Netherlands

E-mail: s.r.parnell@tudelft.nl

Abstract. The spin-echo small-angle neutron scattering (SESANS) technique utilises a series of inclined magnetic fields before and after the sample to encode the scattering angle into the polarisation to obtain a much higher resolution than in conventional SANS. The analogous technique (spin echo modulated SANS (SEMSANS)) implements spin manipulations before the sample only to encode the scattering into an intensity modulation. The technique can be combined with SANS to expand the length scale range probed from 1 nm to microns.

Using McStas we show that using a series of four magnetic Wollaston prisms in two orthogonal pairs with a 90° rotation can be utilised to create SEMSANS modulations in 2-D. These modulations can also be of different periods in each encoding direction. This method can be applied to anisotropic scattering samples. Also this allows for the simultaneous measurement at two orthogonal independent spin-echo lengths. This technique yields directly information about the structure of oriented structures.

1. Introduction

The use of neutron spin-echo [1] is an established technique in neutron scattering for achieving higher resolution than is otherwise possible and without the drawbacks of excessive beam collimation, which often reduces the effective flux to almost unmanageable levels.

In small angle scattering it is possible to reach longer length scales by the techniques of spin-echo SANS (SESANS) [2, 3, 4] and the newer technique of spin echo modulated SANS (SEMSANS) . Both of these techniques utilise magnetic fields with inclined interfaces to encode the scattering angle [8, 9, 10].

However, so far the technique has been largely limited to the investigation of isotropic structures where the scattering is radially symmetric in Q, as is often the case in SANS and there exist only a few instances where samples have been measured in different orientations [13]. Most of these measurements show refraction on oriented wires, fibres and air bubbles [14, 15, 16, 17]. However there are many applications such as rheometry, magnetic scattering, gels and foods where there is orientation of the structures on the nanoscale. In these cases the assumption of isotropic scattering and subsequent radial averaging smears out these structures and also looses important information.

As SESANS and SEMSANS encode the scattering angle via a series of inclined magnetic fields, then the encoding of the scattering is only along the inclination axis of this magnetic

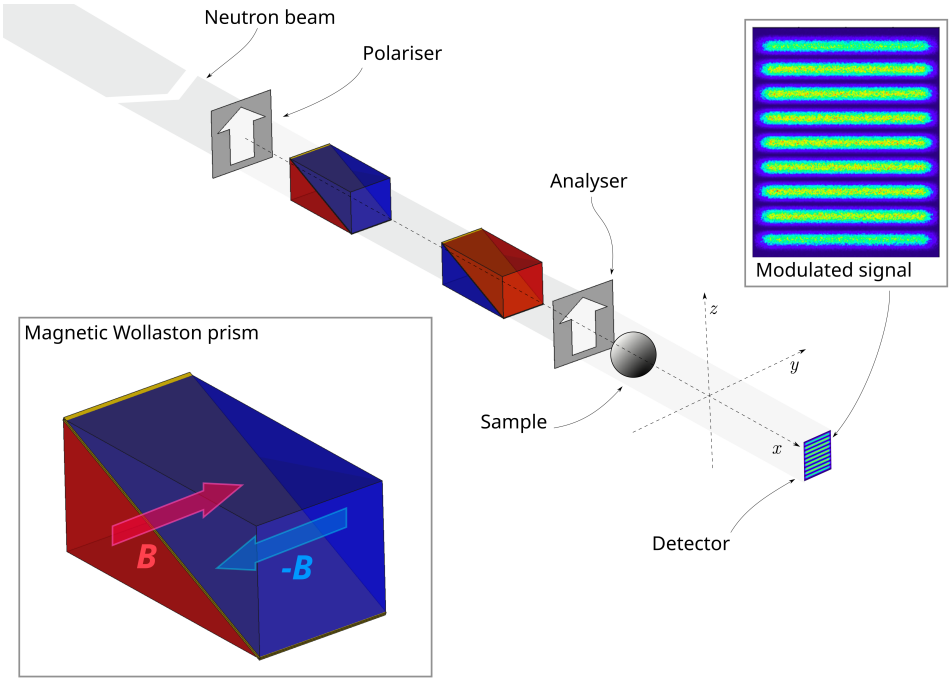

Figure 1. A schematic representation of the general SEMSANS beamline. The neutrons come in from the left after which they are polarised in the +z-direction. The fields in the Wollaston prisms are in the +y and -y-directions. As the second prism is twice as close to the detector as the first prism, the field strength in the second prism is also twice as large. There are also 1cm $\times$ 1cm (rectangular) slits, which are not shown but located at x = 1.9 m and x = 6.1 m

field. The exact arrangements of these fields vary between SESANS and SEMSANS and for the remainder of this article the focus is on the SEMSANS method.

A typical SEMSANS setup is shown in figure 1 where the magnetic fields are generated by a pair of magnetic Wollaston prisms (MWPs)[18], for a complete overview of the prisms the reader is directed to [19] and references therein. The SEMSANS setup has been recently simulated [22] in McStas [23, 24, 25, 26, 27] for a series of inclined permalloy foils [11], not only is the actual spatial modulation of the beam simulated, the resulting correlation function is also obtained for a sample of dilute spheres.

The structure of the remainder of this article is as follows, first is a short introduction to 1-D SEMSANS and the measured correlation function and the relationship between SANS and SEMSANS, followed by simulations of various instrumental configurations. We finish by discussing practical setups and implementation.

2. 1-D SEMSANS

The regular SEMSANS setup is shown in figure 1 and is used to produce a spatially modulation of the intensity focused at the detector [8]. This has been discussed at length in [9] and we summarise from that paper, for more detail the reader is directed to this paper.

For a fixed neutron wavelength and geometry the period (p) of the modulation at the focus (detector) is given by;

$$p = \frac{\pi \tan\theta}{c\lambda(B_2 - B_1)} \tag{1}$$

where c is a constant with a value of $4.62 \times 10^{14} rad \cdot T^{-1} \cdot m^{-2}$ and θ the angle between the hypotenuse in the MWPs and the x axis (as defined in Figure 1), which for the MWP used in these simulations is 45°. With B_1 and B_2 being the magnetic field strength in the first and second MWPs. This arrangement creates a spatial modulation of the neutron intensity along the y direction given by

$$I_{b,s}(y) = \pm A_{b,s} \cos\left(\frac{2\pi}{p} y + \phi\right) + \bar{I}_{b,s} \tag{2}$$

where the sign of " ± " is determined by the choice of incident beam polarisation, $A_{b,s}$ and $\bar{I}_{b,s}$ are the amplitude and average intensity of the spatial intensity modulations respectively and b and s refer to blank and sample respectively. ϕ is an offset phase dependent upon the instrumental settings, which can be adjusted by varying the magnetic guide field between the magnetic Wollaston prisms in an experimental setup. However in this simulation as there is no extraneous magnetic field $\phi = 0$. The accessible length scale of the SEMSANS setup is given by the spin echo length δ, which is determined by the period of the intensity modulation on the detector (p) along with the distances from the sample to the detector plane (L_s) and neutron wavelength (λ) [8];

$$\delta = \lambda L_s / p \tag{3}$$

The quantity measured $A_n(\delta)$ is determined by the ratio of the intensity modulation with $A_s(\delta)$ and without sample $A_b(\delta)$ as a function of spin echo length (δ) and assuming that all scattered neutrons arrive at the detector [19] is given by;

$$A_n(\delta) = e^{\sigma[G(\delta)-1]} \tag{4}$$

where σ is the average number of times a neutron scatters when traversing the sample, which takes into account multiple scattering.

$G(\delta)$, which is the correlation function, is given by;

$$G(\delta) = \frac{1}{\sigma k_0^2} \int_{Q_{zmin}}^{Q_{zmax}} \int_{Q_{ymin}}^{Q_{ymax}} \frac{d\sigma}{d\Omega}(Q) \cos\left(Q_y \delta\right) dQ_y dQ_z \tag{5}$$

where k_0^2 is the square of the incoming neutron wave vector, the Q_y and Q_z directions are as defined in Figure 1. For a simple sample of spheres this shows a correlation function which starts at unity and decays at a value corresponding to twice the radius (as show in in figure 3). It should be noted that this is the case for a dilute system and as expected only correlations within individual spheres are observed and no inter-particle correlations.

The quantity $\frac{d\sigma}{d\Omega}(Q)$ is the neutron scattering cross section per unit volume of sample and equation 5 shows the relationship between SESANS and SANS. This is different from many recent treatments such as [20] and [21] where isotropic scattering is assumed and hence the Hankel transform can be applied.

The setup shown in figure 1 is for a 1-D SEMSANS setup and is simple to implement in McStas, we utilised the McStas script package to this along with the Wollaston prism model developed in our earlier work [29]. This module is based on a finite element simulation of a superconducting prism. The fields are described by polynomials derived from a finite elements simulation using the MagNet (Infolytica, US) software. Hence this gives a realistic field integral for any path of the neutron through the device. It should be noted that whilst in experiments we implement a $\pi/2$ rotation to project the neutron spin into the encoding plane we simply initialise the polarisation in this plane using the perfect polariser McStas component and likewise do the same for the analyser to project only the required component to the detector.

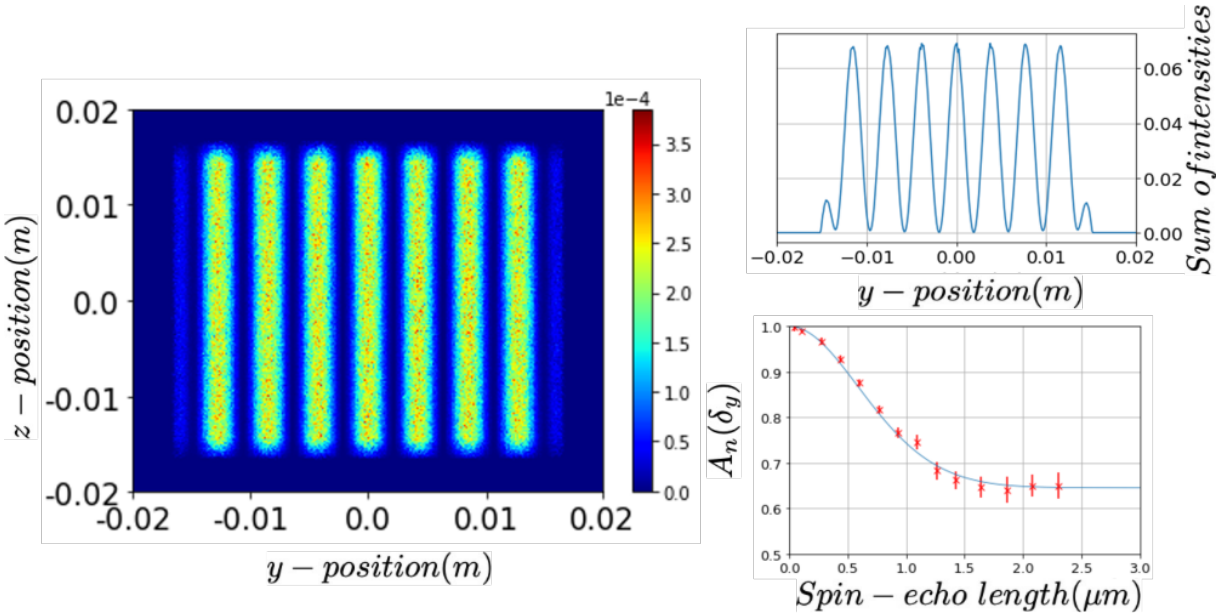

Figure 2. Shown on the left are the intensities on the PSD screen and the corresponding vertical integration (right top) for simulations run on the 1-D SEMSANS beamline. On the bottom right are the derived visibilities for a dilute sphere as a function of spin echo length and also the corresponding analytical expected form for a 2 micron dilute sphere. The instrument was simulated in all cases for $\lambda = 2.36$Å with a wavelength spread of $\Delta\lambda = 0.05$ Å and magnetic field strength of $\Delta B = 7.5$ mT between the two Wollaston prisms. A total of 10^8 neutrons were simulated with a flux of 10^8 n/s/Å/cm^2.

The results of the 1-D SEMSANS simulation are shown in figure 2. On the left is a typical intensity variation which shows the characteristic spatial intensity modulation at the detector and on the right is the resulting periodicity which is obtained along the y-axis. This expected behaviour gives good agreement with the period predicted by equation 2. The results are also in agreement with the McStas simulations of the system with magnetised foils [22]. It should be noted though that the intensity decreases at the edges of the detector. This is due to the finite size of the source, combined with slits before each prism which serve to define the beam within the active are of the MWPs.

The function of these simulations of the 1-D SEMSANS setup is only to establish the validity of the method, check that these simulations work using MWP's and that good agreement is found from the resulting correlation function.

3. 2-D SEMSANS

As we have already discussed the 'standard' SEMSANS method is 1-D and sensitive only to correlations along the encoding axis. There have been a number of suggestions to encode using different schemes [30, 31], however the approach which we describe below utilises the already existing technology of MWPs and does not need additional magnetic field component development.

In order to create encoding in two directions we need to create two encoding axes, hence we need to modify the modulation given by equation 2 to give an additional modulation in the z

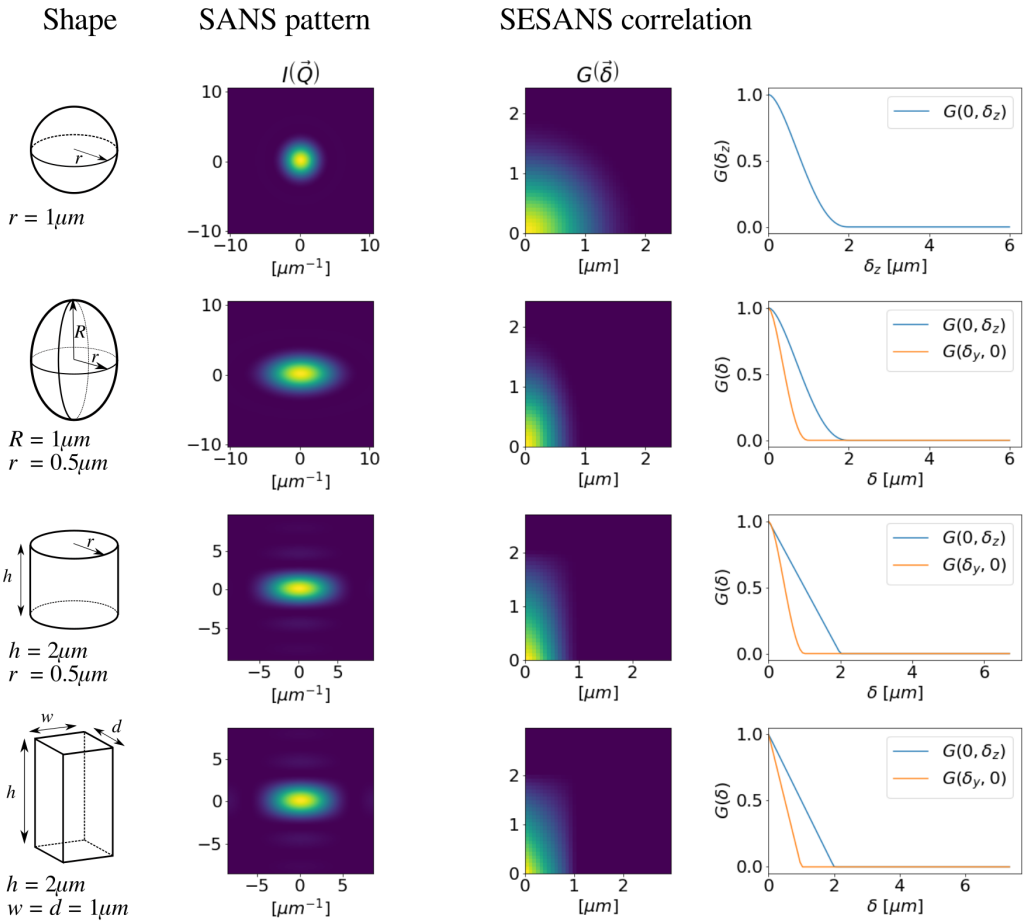

Figure 3. Shown in the left column are the various shapes along with dimensions for the simulated nanoparticles, the second column is the corresponding SANS scattering as a function of momentum transfer (Q). The third column if the corresponding SEMSANS correlation function in 2-D and the fourth column is the projection of that correlation function along a given axis. Note that the coordinate frame is consistent with the SEMSANS setup diagram as shown in figures 1 and 4.

direction given by;

$$I_{b,s}(y,z) = \pm A_{b,s} \cos\left(\frac{2\pi}{p_y} y + \phi\right) \cos\left(\frac{2\pi}{p_z} z + \phi\right) + \bar{I}_{b,s} \tag{6}$$

where the periods in y and z are given by p_y and p_z respectively and hence the correlation function is now given by;

$$G(\delta_y, \delta_z) = \frac{1}{\sigma k_0^2} \int_{Q_{zmin}}^{Q_{zmax}} \int_{Q_{ymin}}^{Q_{ymax}} \frac{d\sigma}{d\Omega}(Q) cos(Q_y \delta_y) cos(Q_z \delta_z) dQ_y dQ_z \tag{7}$$

Examples of these two orthogonal correlation functions are shown in figure 3 for a range of anisotropic nanoparticles, these show that the measured correlation function is indeed different,

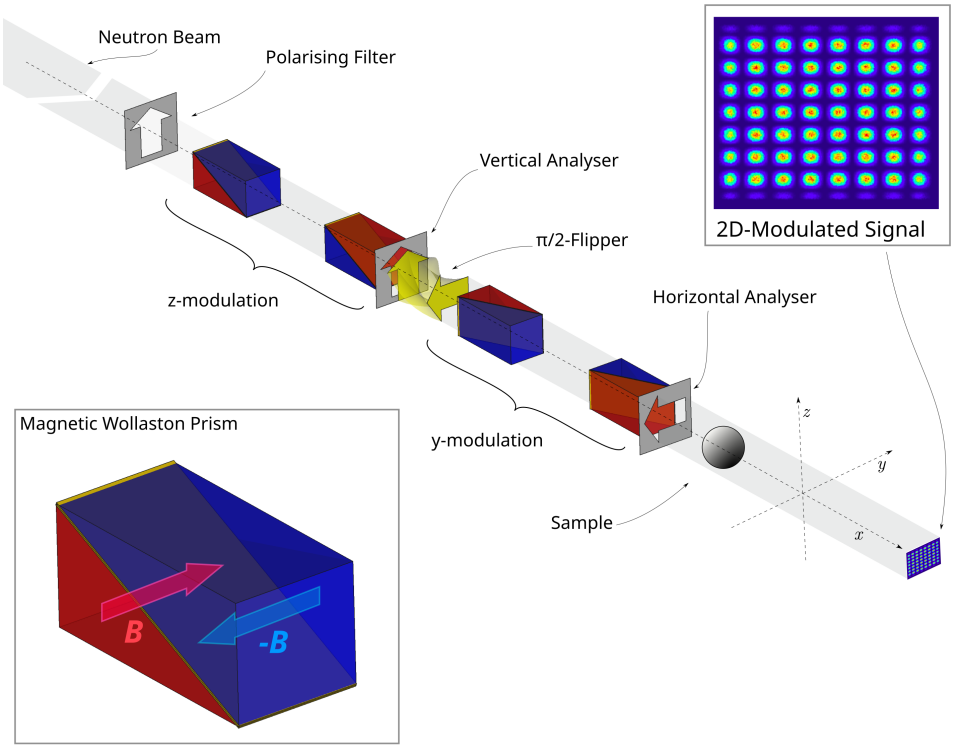

Figure 4. The proposed new scheme to generate modulation in the x and y directions. In this set-up, the order in which we construct the two prism sets is changed: the first prism set, for modulation in y, consists of the first two prisms and the second prism set is composed by the last two prisms, which makes sure there is modulation in the z direction. To circumvent the problem of losing modulation depth the neutrons enter the first prism set with a z-polarisation, after which they are analysed in the same direction. Hereafter, in order to obtain full modulation depth, the neutron beam must be polarised in the y-direction when entering the last prism set.

as expected. We have introduced the nomenclature δ_i where $i = y, z$ defined by the particular encoding axis.

The question now arises as to how to achieve these modulations. The scheme that we propose is shown schematically in figure 4, this utilises two pairs of MWPs orthogonal to one another with a simple rotation of the magnetic field between the two sets of prisms and the addition of an analyser after the first MWP pair. For this setup the magnetic fields are chosen for each of the two different focusing conditions, one for each prism pair, such that both of the modulations are focused at the detector.

The resulting simulation is shown in figure 5 and is the resulting modulation for two identical spin echo lengths is shown in the top left, the resulting pattern can be collapsed (integrated) along either the y or z directions (top right) and shows a high degree of visibility, note that in this case both spin states (I_+ and I_-) were simulated and the resulting visibility derived assuming the usual definition of neutron visibility (which is defined by the two neutron polarisation spin states) ($V = (I_+ - I_-)/(I_+ + I_-)$). In order to test the effectiveness of this approach we then derive the resulting change in correlation function using equation 4 to get $A_n(\delta)$.

The resultant correlation function shows good agreement with the analytical form given by [32]. When the periods are changed relative to y and z as shown in figure 6 a high modulation depth is achieved again in both the y and z directions. Again the correlation function ($A_n(\delta)$)

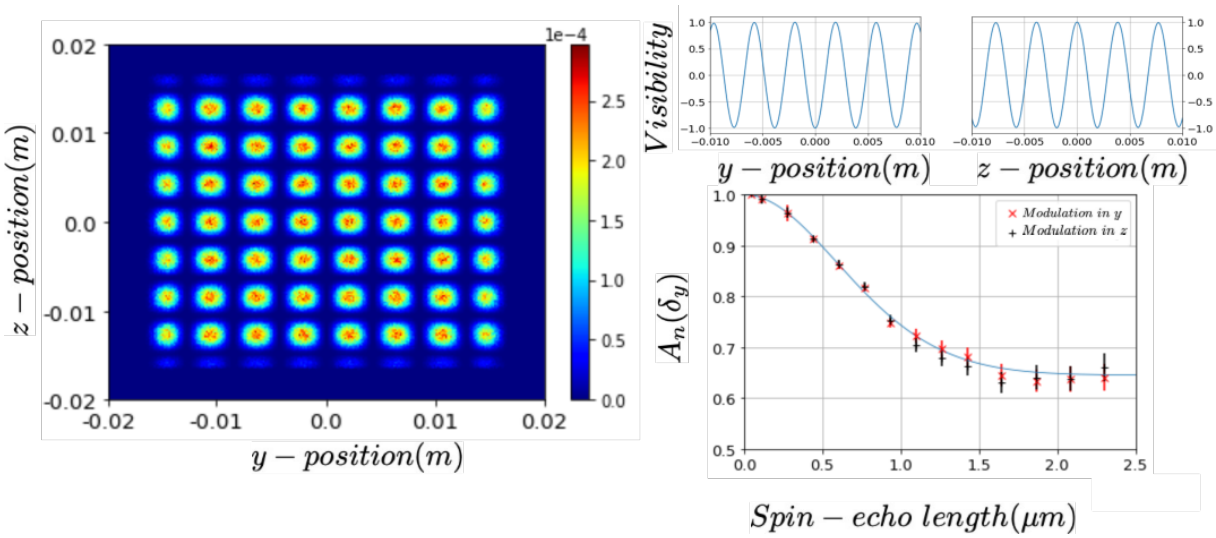

Figure 5. Shown left is an example of the 2-D intensity modulation obtained at the detector position without a sample. Whilst on the top left are the visibility along the y and z directions, this is obtained by integrating across each orthogonal direction. Shown in the bottom right panel is the simulated intensity modulation for dilute spheres measured along the y and z directions.

is derived, showing good agreement for the analytical function.

4. Discussion and further work

The simulations shown in this proceedings suggest that a 2-D modulation using the SEMSANS method is possible. In terms of a physical realisation of this setup, the MWP's can be mounted orthogonally in pairs. Due to the low level of magnetic field aberrations [18] using a series of prisms would have little effect on the resulting depth of modulation. The only limit would be upon the strength of the magnetic field possible to reach relevant spin echo length scales in the micron region.

Such a system would need a suitable detector and the existing designs such as the multi channel plate detectors [33] have high pixel density ($55\mu m$) in two dimensions allowing high resolution determination of the modulation depth. In addition to the multi channel plate detectors there are also promising implementations of Anger cameras for neutrons [34] with high spatial resolution.

These simulations were for a simple monochromatic instrument, however conceptually there is no reason why such an implementation could not also be adapted to time of flight based setups. The detector systems mentioned in the previous paragraph can also be used in time of flight mode with high time resolution as was done in [7]. It could be possible to incorporate this within the SEMSANS - SANS instrument concept as well, however this would require a smaller detector such that it can be mounted in the beamstop area and not interfere with the 2-D SANS detector. Ideally for SEMSANS-SANS the analyser may provide more parasitic scattering and may need to be replaced with a ^{3}He analyser, which is becoming routine in time of flight scattering now [35, 28]. In particular with almost no background when using silicon windowed cells.

It should also be mentioned that variants upon this technique can also be employed in an imaging configuration [36].

One advantage in advancing these simulations would be to incorporate an anisotropic scatterer within the McStas sample modules to approximate some of the nanoparticle geometries

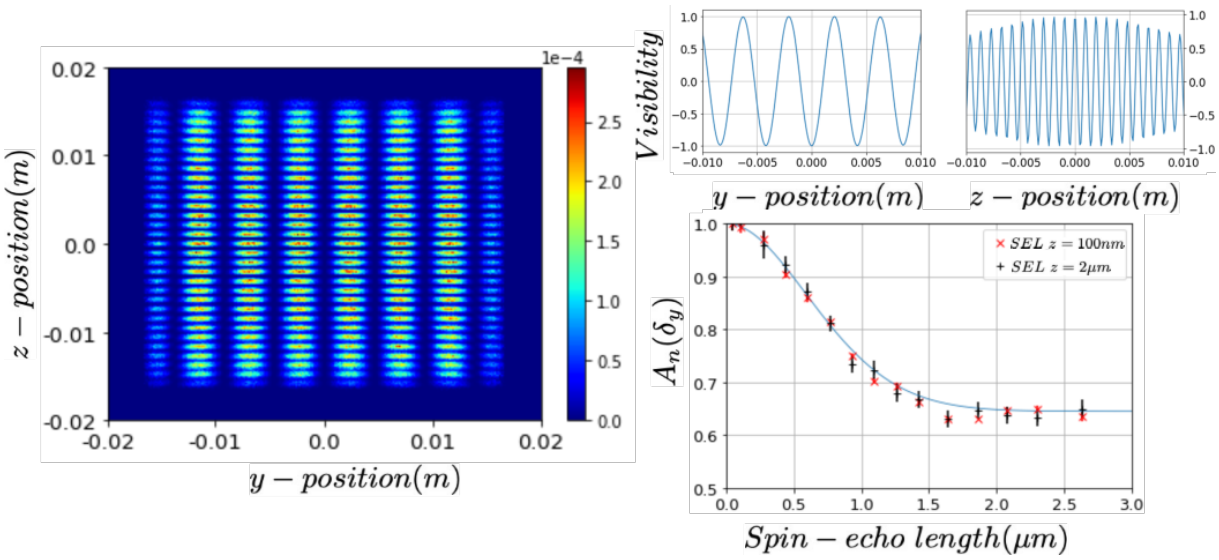

Figure 6. Shown left is an example of the 2-D intensity modulation obtained at the detector position without a sample. Whilst on the top left are the visibility along the y and z directions, this is obtained by integrating across each orthogonal direction. The magnetic field strength was ΔB=7.5mT between the first prism set and 6.9mT between the second pair. Shown in the bottom right panel is the simulated intensity modulation for dilute spheres measured along the y and z directions with different periods and hence spin echo lengths (SEL) probed. Note that the SEL along z is fixed (as indicated in the legend) whilst the SEL in y is scanned with the magnetic fields being ΔB = 3, 7.5, 19, 30, 41, 52, 64, 75, 87, 98, 113, 128, 143, 158, 180 mT.

shown in figure 3.

5. Conclusions

We have shown via Monte Carlo simulations an implementation of a 2-D SEMSANS measurement. The results show that such a setup is feasible and can be implemented using the existing hardware that has been developed. Such a setup could be used for anistotropic scatterers. This could also be used for magnetic scattering. The proposed setup uses existing components and does not need the development of new polarisation optics and can be implemented on existing setups.

6. Acknowledgements

The authors are grateful to the McStas team for help with the simulations, also to Mads Bertelsen who developed McStasScript and helped with the installation and implementation. We would like to thank Fankang Li from Oak Ridge National Laboratory who created the magnetic Wollaston prism component in McStas based on his MagNET simulations and we acknowledge conversations with Roger Pynn from Indiana University Bloomington.

References

[1] Neutron Spin Echo Spectroscopy, Lecture Notes in Physics, Vol. 601, edited by F. Mezei, C. Pappas and T. Gutberlet, Berlin, Heidelberg: Springer.
[2] M. T. Rekveldt, Nucl. Instrum. Methods Phys. Res., Sect. B 114, 366 (1996)
[3] M.T. Rekveldt, J. Plomp, W.G. Bouwman, W.H. Kraan, S. Grigoriev, M. Blaauw, Rev. Sci. Instrum. 76 (3) (2005) 033901.

[4] S.R. Parnell, A.L. Washington, K. Li, H. Yan, P. Stonaha, F. Li, T. Wang, A. Walsh, W.C. Chen, A.J. Parnell, J.P.A. Fairclough, D.V. Baxter, W.M. Snow, R. Pynn, Rev. Sci. Instrum. 86 (2) (2015) 023902.
[5] M. Strobl, A. S. Tremsin, A. Hilger, F. Wieder, N. Kardjilov, I. Manke, W. G. Bouwman, and J. Plomp , Journal of Applied Physics 112, 014503 (2012)
[6] M. Strobl and F. Wieder and C.P. Duif and A. Hilger and N. Kardjilov and I. Manke and W.G. Bouwman, Physica B 407 (2012) 4132-4135
[7] F.Li, S.R.Parnell, R.M.Dalgliesh, A.Washington, J.Plomp and R.Pynn, Scientific Reports (2019) 9:8563
[8] W.G.Bouwman, C.P.Duif and R. Gähler, Physica B 404 (2009) 25850–2589.
[9] W.G. Bouwman, C.P. Duif, J. Plomp, A. Wiedenmann, R. Gähler, Physica B 406 (12) (2011) 2357–2360.
[10] F. Li, S.R. Parnell, H. Bai, W. Yang, W.A. Hamilton, B.B. Maranville, R. Ashkar, D.V. Baxter, J.T. Cremer, R. Pynn, Journal of Applied Crystallography, 49 (1) (2016) 55–63.
[11] W.H.Kraan and M.T.Rekveldt, Nuclear Instruments and Methods A, 596 (2008) 422-429.
[12] S.R. Parnell, R.M. Dalgliesh, N.J. Steinke, J. Plomp and A.A. Van Well, Journal of Physics Conference Series, 1021, 012040, (2018)
[13] Burg, S.L., Washington, A., Coles, D.M. et al., Communications Chemistry 2, 100 (2019).
[14] W.G. Bouwman, T.V. Krouglov, J. Plomp, S.V. Grigoriev, W.H. Kraan, M.Th. Rekveldt, Physica B, 350 (2004) 140–146
[15] J. Plomp, J.G. Barker, V.O. De Haan, W.G. Bouwman, A.A. van Well, Nuclear Instruments and Methods A 574 (2007) 324–329
[16] G.A. Krintiras, J.Göbel, W.G. Bouwman, A.J. van der Goot, G.D. Stefanidis, Food & function 5 (2014) 3233–3240
[17] B. Tian, Z. Wang, A.J. van der Goot, W.G. Bouwman, Food Hydrocolloids 83 (2018) 287–295
[18] F. Li, S.R. Parnell, W.A. Hamilton, B.B. Maranville, T. Wang, R. Semerad, D.V. Baxter, J.T. Cremer, R. Pynn, Review of Scientific Instruments 85 (5) (2014).
[19] F.Li, Nina -J. Steinke, Robert M. Dalgliesh, Adam L. Washington, Jiazhou Shen, Roger Pynn, Steven R. Parnell, Nuclear Instruments and Methods A, 1014 (2021) 165705
[20] Jurrian H. Bakker, Adam L. Washington, Steven R. Parnell, Ad A. van Well, Catherine Pappas and Wim G. Bouwman, Journal of Neutron Research, 22 (2020) 57-70
[21] R. Andersson, L.F. Van Heijkamp, I.M. De Schepper, W.G. Bouwman, Journal of Applied Crystallography, 41 (5) (2008) 868–885.
[22] W.G. Bouwman and E.B. Knudsen and L. Udby and P. Willendrup, *Journal of applied Crystallography* **54** (2021), pp. 195–202
[23] K. Lefmann and K. Nielsen, Neutron News 10, 20, (1999).
[24] P. Willendrup, E. Farhi and K. Lefmann, Physica B, 350 (2004) 735.
[25] P. Willendrup, E. Farhi E. Knudsen, U. Filges and K. Lefmann, Journal of Neutron Research, vol. 17, no. 1, pp. 35-43, 2014
[26] P. Willendrup, and K. Lefmann, Journal of Neutron Research, vol. 22, no. 1, pp. 1-16, 2020
[27] P. Willendrup, and K. Lefmann, Journal of Neutron Research, vol. 23, no. 1, pp. 7-27, 2021
[28] J. Schmitt, J.J. Zeeuw, J. Plomp, W.G. Bouwman, A.L. Washington, R.M. Dalgliesh, C.P. Duif, M.A. Thijs, F. Li, R. Pynn, S.R. Parnell, K.J. Edler, ACS Appl. Mater. Interfaces 12 (25) (2020) 28461–28473.
[29] F. Li, S.R. Parnell, T. Wang, D.V. Baxter, R. Pynn, Journal of Physics Conference Series 711 (1) (2016) 012015.
[30] J.Zhao, P.Yuan, Proc. SPIE 4785, Advances in Neutron Scattering Instrumentation, (18 November 2002)
[31] E.Kadletz, W.G.Bouwman and C.Pappas, Journal of Applied Crsytallography, Volume 55 (2022)
[32] T. Krouglov, W. G. Bouwman, J. Plomp, M. T. Rekveldt, G. J. Vroege, A. V. Petukhov and D. M. E. Thies-Weesie, Journal Of Applied Crystallography, (2003). 36, 1417-1423
[33] Tremsin, A. S. et al., Nucl. Instruments Methods Phys. Res. Sect. A: Accel. Spectrometers, Detect. Assoc. Equip. 604, 140–143, 01.041 (2009)
[34] R.A. Riedel, C. Donahue, T. Visscher, C. Montcalm, Nuclear Instruments and Methods A, 794 (2015) 224-233
[35] S.Boag, S.R.Parnell, C.D¿Frost, K.H.Andersen and E.Babcock, Physics B, (2007) 179-181
[36] Markus Strobl, Morten Sales, Jeroen Plomp, Wim G. Bouwman, Anton S. Tremsin, Anders Kaestner, Catherine Pappas, Klaus Habicht, Scientific Reports, (2015) 5, 16576